

RSC Advances



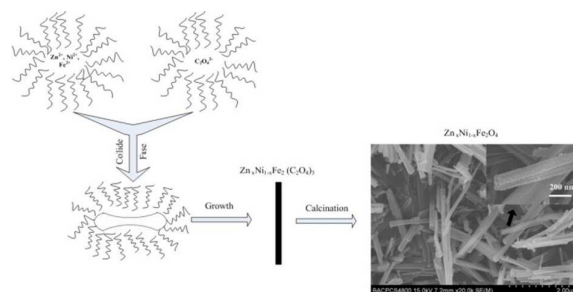
This is an *Accepted Manuscript*, which has been through the Royal Society of Chemistry peer review process and has been accepted for publication.

Accepted Manuscripts are published online shortly after acceptance, before technical editing, formatting and proof reading. Using this free service, authors can make their results available to the community, in citable form, before we publish the edited article. This *Accepted Manuscript* will be replaced by the edited, formatted and paginated article as soon as this is available.

You can find more information about *Accepted Manuscripts* in the [Information for Authors](#).

Please note that technical editing may introduce minor changes to the text and/or graphics, which may alter content. The journal's standard [Terms & Conditions](#) and the [Ethical guidelines](#) still apply. In no event shall the Royal Society of Chemistry be held responsible for any errors or omissions in this *Accepted Manuscript* or any consequences arising from the use of any information it contains.

Zinc–nickel (Zn–Ni) ferrite nanorods were synthesized by a microemulsion-based method in combination with calcination at different temperatures



Synthesis of zinc–nickel ferrite nanorods and their magnetic properties

Liang Hao, Yun Zhao, Qingze Jiao*, Puteng Chen

School of Chemical Engineering and the Environment, Beijing Institute of Technology, Beijing 100081, China

Abstract:

Zinc–nickel (Zn–Ni) ferrite nanorods were synthesized by a microemulsion-based method in combination with calcination at different temperatures. The morphologies and structures of Zn–Ni ferrite nanorods and their precursors of Zn/Ni/Fe composite oxalate nanorods were characterized using a field emission scanning electron microscopy and X-ray diffractometer. Magnetization measurement was carried out using a vibrating sample magnetometer at room temperature. It was shown that the Zn–Ni ferrite nanorods were around 50–200 nm in diameter and several micrometers in length. Their saturation magnetization increased with increasing calcination temperatures from 350 to 900 °C. In addition, the magnetic properties of Zn–Ni ferrite nanorods were also affected by their compositions.

Keywords: Zn–Ni ferrite; Chemical synthesis; Microstructure; Magnetic measurements.

1. Introduction

Soft ferrites are commercially important materials on account of their electrical and magnetic properties[1]. Spinel-type ferrite, with general formula AFe_2O_4 , are widely used in many electronic and magnetic devices because of high magnetic permeability and low magnetic loss[2]. Among them, nickel ferrite ($NiFe_2O_4$) has been intensively investigated as one of the magnetic nanomaterials [3-7]. Recently, doping of inverse spinel ferrites with zinc element are used to improve their electrical or magnetic properties [8-11]. Zinc-nickel (Zn–Ni) ferrite is a versatile ferrite from the viewpoint of its large number of applications due to its high magnetic permeability, high electrical resistivity, high Curie temperature, and low power loss at high frequencies [12-14]. At present, many routes are developed to prepare Zn–Ni ferrite nanoparticles such as thermal decomposition[13], inert gas condensation [14], co-precipitation [15], hydrothermal reaction [16], sol–gel process[17,18] and ball milling [19]. However, few

*Corresponding author. Fax: +86 10 68918979. E-mail address: jiaoqz@bit.edu.cn (QZ . Jiao).

reports involve the one-dimensional (1D) Zn-Ni ferrite nanomaterials. Wu et al. [20] reported that Zn/Ni/Fe composite oxide nanotubes with length of 1 to 5 μm and outer diameter of 200 nm showed 60 Oe of coercivity and 0.6 emu/g of largest magnetocrystalline magnetization. The properties of ferrites are known to be strongly influenced by the composition, size, morphology and microstructures [21]. With no doubt, Zn-Ni ferrite nanorods are expecting to show unique magnetic properties.

In this work, we report the synthesis of Zn-Ni ferrite nanorods with various magnetic properties. This was achieved by calcination of precursors with different molar ratio of Zn, Ni and Fe, prepared using a coprecipitation reaction of Zn^{2+} , Ni^{2+} and Fe^{3+} with $\text{H}_2\text{C}_2\text{O}_4$ in a microemulsion solution.

2. Experimental

2.1. Preparation of Zn-Ni ferrite nanorods

A microemulsion system consisting of cetyltrimethylammonium bromide (CTAB)/water/cyclohexane/n-pentanol was selected for synthesis of $\text{Zn}_x\text{Ni}_{1-x}\text{Fe}_2(\text{C}_2\text{O}_4)_3$ precursors. The microemulsion was prepared by dissolving CTAB (1.0 g) in a mixture of 75 ml of cyclohexane and 2.5 ml of n-pentanol. The resulting solution was stirred for 30 min. Subsequently, 3.75 ml of an oxalic acid ($\text{H}_2\text{C}_2\text{O}_4$) aqueous solution (1.2 M) was added into the above solution and the mixture was stirred for an additional 1 h. 1.25 ml of an aqueous solution containing $\text{ZnSO}_4[0.4x\text{ M}]$, $\text{NiSO}_4[(1-x)0.4\text{ M}]$ ($x = 0-1$) and $\text{FeSO}_4(0.8\text{ M})$ was then added to the above microemulsion and stirred for 24 h at room temperature. The as-synthesized solid $\text{Zn}_x\text{Ni}_{1-x}\text{Fe}_2(\text{C}_2\text{O}_4)_3$ precursor was washed with alcohol and distilled water, centrifuged, and dried. Finally, $\text{Zn}_x\text{Ni}_{1-x}\text{Fe}_2\text{O}_4$ nanorods were obtained by calcination of the precursor at different temperatures for 3 h.

2.2. Characterization

Energy-dispersive X-ray spectroscopy (EDS) and field emission scanning electron microscopy (FESEM) were performed with a Hitachi S-4800 microscope operated at 15 kV. Thermal gravimetric analysis (TGA) was carried out on a SEIKO TG/DTA6200 thermal analyser at a heating rate of 10 K min^{-1} from room temperature to $800\text{ }^\circ\text{C}$ in air. Powder X-ray diffraction (XRD) patterns were recorded on a X-ray diffractometer (Rigaku Ultima IV) at 40 kV and 40 mA with Cu K α radiation. The magnetic properties were measured using a Lakeshore 7300 vibrating sample magnetometer (VSM).

3. Results and discussion

3.1. Morphology and structure of Zn/Ni/Fe composite oxalate nanorods

Fig. 1 shows SEM image and EDS spectrum of $\text{Zn}_{0.5}\text{Ni}_{0.5}\text{Fe}_2(\text{C}_2\text{O}_4)_3$ nanorods. As shown in Fig. 1(a), $\text{Zn}_{0.5}\text{Ni}_{0.5}\text{Fe}_2(\text{C}_2\text{O}_4)_3$ nanorods are around 50–200 nm in diameter and several micrometers in length. The SEM image also reveals that the surface of the rods is very smooth. By observation of the EDS spectrum of the nanorods (Fig. 1(b)), only Zn, Ni, Fe, C and O are detected, which further confirms the formation of pure $\text{Zn}_{0.5}\text{Ni}_{0.5}\text{Fe}_2(\text{C}_2\text{O}_4)_3$ nanorods. Fig. 2 shows XRD patterns of the four different oxalate nanorods prepared at similar conditions. The diffraction peaks of Zn/Ni/Fe composite oxalate (Fig. 2a) are different from those of any other three single metal oxalate (Fig. 2b, c, and d) and not the simple superposition of b, c and d, implying that the structure of the precursor is Zn/Ni/Fe composite oxalate like $\text{Zn}_{0.5}\text{Ni}_{0.5}\text{Fe}_2(\text{C}_2\text{O}_4)_3$.

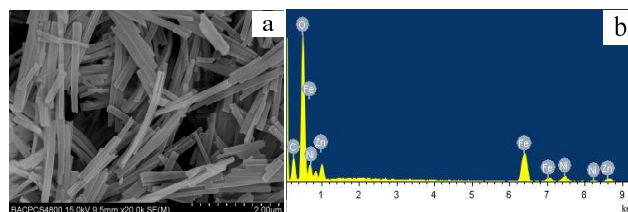


Fig. 1. Morphology and composition of the $\text{Zn}_{0.5}\text{Ni}_{0.5}\text{Fe}_2(\text{C}_2\text{O}_4)_3$ nanorods prepared by a microemulsion-based method: (a) SEM image, (b) EDS spectrum.

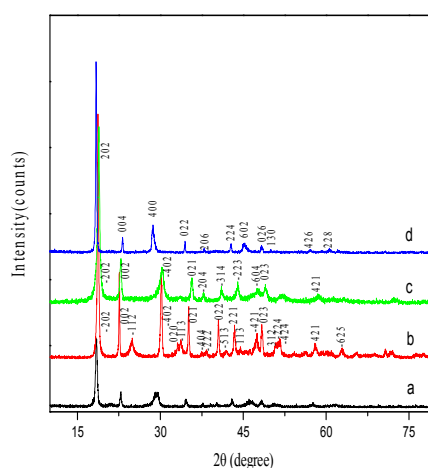


Fig. 2. XRD patterns of the different oxalate nanorods: (a) $\text{Zn}_{0.5}\text{Ni}_{0.5}\text{Fe}_2(\text{C}_2\text{O}_4)_3$, (b) ZnC_2O_4 , (c) NiC_2O_4 , and (d) FeC_2O_4 .

3.2. Thermal property of Zn/Ni/Fe composite oxalate nanorods

As shown in Fig. 3, the thermal behavior of Zn/Ni/Fe composite oxalate nanorods is characterized by two transitions: the first

one at low temperature corresponds to the loss of surface water; the second one at higher temperature (180–320 °C) is due to decomposition of the oxalate. Therefore Zn–Ni ferrite nanorods can be obtained by calcining oxalate precursors at higher than 320 °C based on this TGA curve.

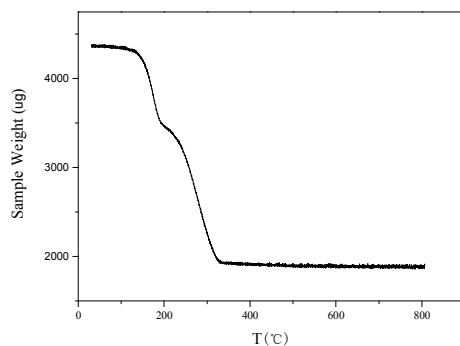


Fig. 3. TGA curve of Zn/Ni/Fe composite oxalate nanorods.

3.3. Morphology and structure of Zn–Ni ferrite nanorods

SEM images of $\text{Zn}_{0.5}\text{Ni}_{0.5}\text{Fe}_2\text{O}_4$ nanorods by calcination of the precursors at different temperatures (350, 500, 650, 800 and 900 °C) are shown in Fig. 4. Fig. 4a shows $\text{Zn}_{0.5}\text{Ni}_{0.5}\text{Fe}_2(\text{C}_2\text{O}_4)_3$ precursor nanorods which are characterized by the smooth surface morphology. After calcination, the products retain original rodlike morphology of the precursor and the $\text{Zn}_{0.5}\text{Ni}_{0.5}\text{Fe}_2\text{O}_4$ nanorods are formed by nanoparticles. It can be concluded that the formation of the $\text{Zn}_{0.5}\text{Ni}_{0.5}\text{Fe}_2\text{O}_4$ nanorods during the calcination process was restricted within the $\text{Zn}_{0.5}\text{Ni}_{0.5}\text{Fe}_2(\text{C}_2\text{O}_4)_3$ template. In other words, this growth process can be viewed as a morphologically templated nucleation process [22]. As shown in Fig. 4b, the $\text{Zn}_{0.5}\text{Ni}_{0.5}\text{Fe}_2\text{O}_4$ nanorods obtained at 350 °C start to crystallize as the precursor $\text{Zn}_{0.5}\text{Ni}_{0.5}\text{Fe}_2(\text{C}_2\text{O}_4)_3$ begins to decompose into $\text{Zn}_{0.5}\text{Ni}_{0.5}\text{Fe}_2\text{O}_4$ but the nanoparticles are too little to be observed. Fig. 4c shows the SEM image of the nanorods prepared at 500 °C, small $\text{Zn}_{0.5}\text{Ni}_{0.5}\text{Fe}_2\text{O}_4$ nanoparticles are clearly visible. At 650 and 800 °C (Fig. 4d and e), the nanoparticles are now much larger and the number of particles is much lower, indicating an Ostwald ripening and “oriented attachment” processes and the rods are still two micrometers in length. At 900 °C, the $\text{Zn}_{0.5}\text{Ni}_{0.5}\text{Fe}_2\text{O}_4$ nanorods consist of individual crystals bound to each other.

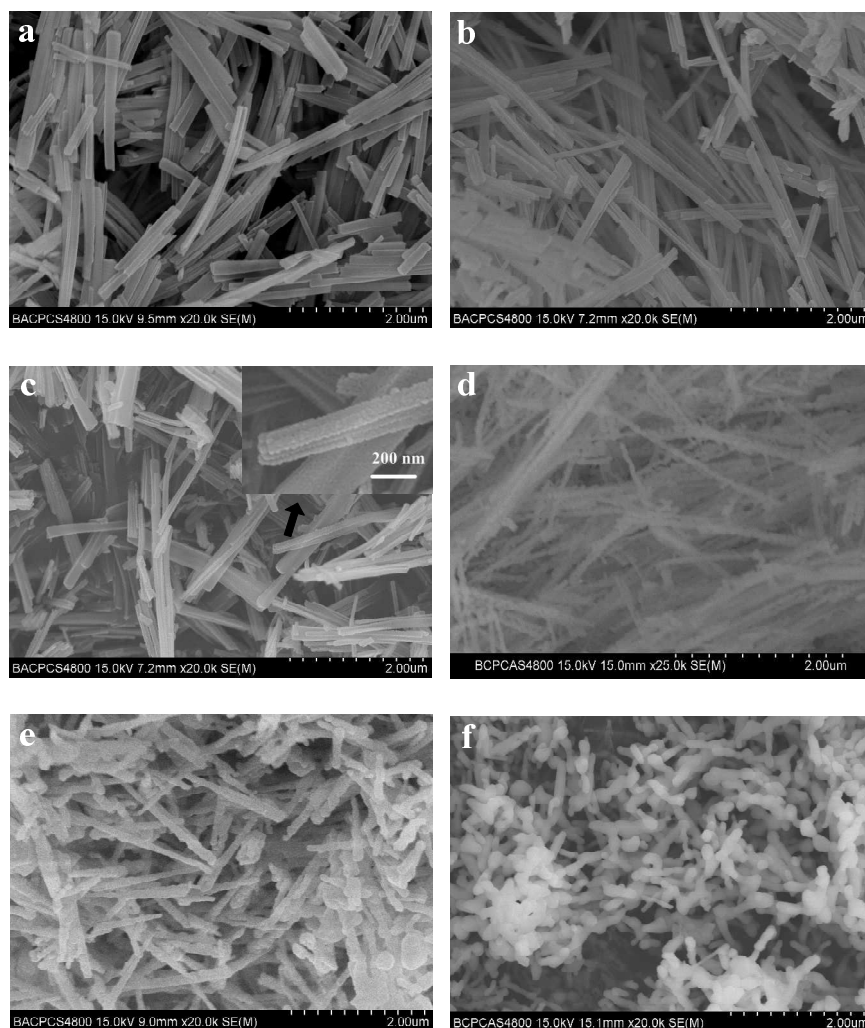


Fig. 4. (a) SEM image of $\text{Zn}_{0.5}\text{Ni}_{0.5}\text{Fe}_2(\text{C}_2\text{O}_4)_3$ nanorods; ((b)–(f)) SEM images of $\text{Zn}_{0.5}\text{Ni}_{0.5}\text{Fe}_2\text{O}_4$ nanorods obtained at different temperatures, (b) 350 °C, (c) 500 °C, (d) 650 °C, (e) 800 °C and (f) 900 °C.

Fig. 5 shows XRD patterns for the $\text{Zn}_{0.5}\text{Ni}_{0.5}\text{Fe}_2\text{O}_4$ nanorods prepared by decomposition of the precursor at 350, 500, 650, 800 and 900 °C respectively. It can be seen that the **inverse** spinel ferrite of $\text{Zn}_{0.5}\text{Ni}_{0.5}\text{Fe}_2\text{O}_4$ is formed as a single phase at all temperatures. All the diffraction peaks can be indexed as pure cubic phase of zinc–nickel ferrite ($\text{Zn}_{0.5}\text{Ni}_{0.5}\text{Fe}_2\text{O}_4$). The intensity of the diffraction peaks of $\text{Zn}_{0.5}\text{Ni}_{0.5}\text{Fe}_2\text{O}_4$ increases and the peak width (full width at half maximum) decreases with increasing calcinations temperatures. This indicates that, as expected and observed, both the crystallinity and the average size of the crystallites increase with increasing calcination temperatures.

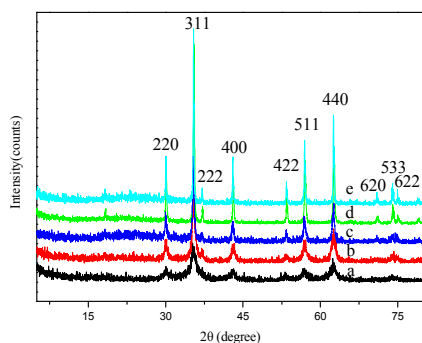


Fig. 5. XRD patterns of $\text{Zn}_{0.5}\text{Ni}_{0.5}\text{Fe}_2\text{O}_4$ nanorods prepared by calcination of the corresponding precursors at different temperatures (a) 350 °C, (b) 500 °C, (c) 650 °C, (d) 800 °C and (e) 900 °C.

Fig. 6 shows SEM images of the $\text{Zn}_x\text{Ni}_{1-x}\text{Fe}_2\text{O}_4$ nanorods with different x values. They are all obtained by decomposition of the precursors at 500 °C. The SEM images show rodlike morphology formed by nanoparticles and the diameter decreases with increasing Zn content. Chemical formulas for $\text{Zn}_x\text{Ni}_{1-x}\text{Fe}_2\text{O}_4$ nanorods are given in Table 1 based on the metal analysis data. Zn/Ni/Fe molar ratios for all samples are consistent with those used in the starting solutions, indicating the complete precipitation of metal ions.

Table 1. Measurement ratio of the metal elements of $\text{Zn}_x\text{Ni}_{1-x}\text{Fe}_2\text{O}_4$ nanorods

Sample	x value	Zn : Ni : Fe
$\text{Zn}_x\text{Ni}_{1-x}\text{Fe}_2\text{O}_4$	0.1	0.08 : 0.85 : 2
	0.35	0.31 : 0.62 : 2
	0.5	0.54 : 0.44 : 2
	0.65	0.60 : 0.39 : 2
	0.9	0.86 : 0.07 : 2

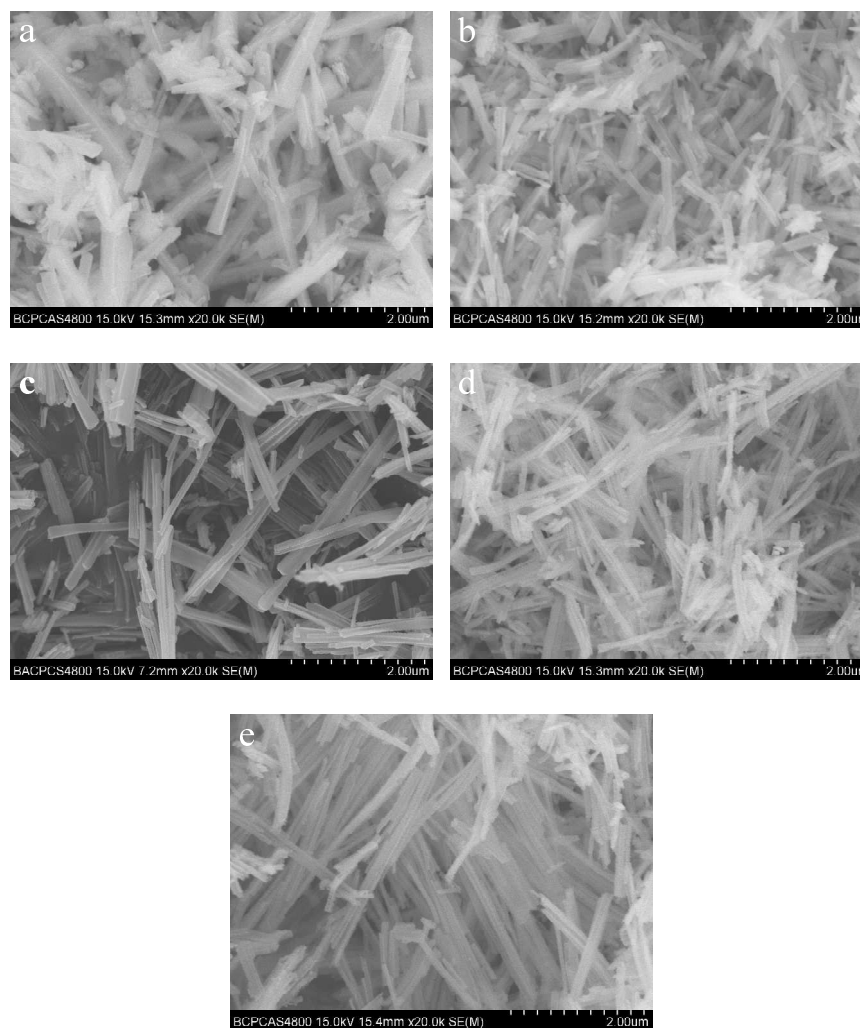


Fig. 6. SEM image of the $Zn_xNi_{1-x}Fe_2O_4$ nanorods with different x values, (a) 0.1, (b) 0.35, (c) 0.5, (d) 0.65, and (e) 0.9

3.4. Magnetic properties of Zn–Ni ferrite nanorods

Fig. 7 shows magnetic hysteresis loops of $Zn_xNi_{1-x}Fe_2O_4$ ($x=0.5$) nanorods prepared by calcination of the precursors at different temperatures. The saturation magnetization (M_s) are summarized in Table 2. The M_s gradually increases with increasing calcination temperatures, or more precisely the crystallite size of the particles. The sample prepared at 350 °C exhibits a narrower hysteresis loop in the M–H curve with M_s of 17.8 emu/g. While in case of the $Zn_xNi_{1-x}Fe_2O_4$ ($x=0.5$) nanorods obtained at 900 °C, the M_s remarkably increases to 77.1 emu/g. Combined with XRD and SEM results, we suggest that well crystallinity and large nanoparticle size of the sample due to the higher temperature aroused the significant increase of M_s . The lower M_s associated to the particles with smaller sizes can be attributed to two reasons. First, surface distortions due to the interaction of the transition metal ions with the oxygen atoms in the spinel lattice can reduce the net magnetic moment in the particle. This effect is especially

prominent for the ultrafine particles due to their large surface to volume ratio [23]. Second, the magnetocrystalline anisotropy of the particles is dependent on the crystallinity of the nanoparticles. As shown in the XRD patterns, samples prepared by decomposition of the precursor at lower temperatures exhibit the lower intensity and crystallinity. Hence, a large proportion of crystal defects and dislocations can occur within the lattice and this will cause a significant reduction of magnetic moment within the particles, as a result of the magnetocrystalline anisotropy distortion.

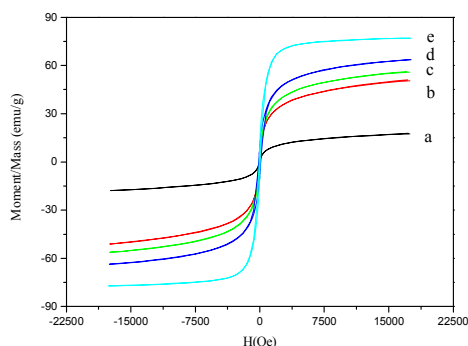


Fig. 7. Magnetic hysteresis loops for $Zn_xNi_{1-x}Fe_2O_4$ ($x=0.5$) nanorods prepared by calcinations of the precursor at different temperatures, (a) 350 °C, (b) 500 °C, (c) 650 °C, (d) 800 °C and (e) 900 °C.

Table 2. Magnetic parameters for $Zn_xNi_{1-x}Fe_2O_4$ ($x=0.5$) nanorods prepared by calcination of the precursor at different temperatures

Temperature (°C)	Ms (emu/g)
350	17.8
500	51.1
650	56.3
800	63.6
900	77.1

Fig. 8 shows hysteresis loops of $Zn_xNi_{1-x}Fe_2O_4$ nanorods with different x values obtained at 500 °C. As shown in Table 3, $Zn_xNi_{1-x}Fe_2O_4$ nanorods with different x values show Ms of 9.3–51.1 emu/g due to different compositions. When Zn doping level (x value) increases from 0.1 to 0.5, the Ms of samples increases. However with further increasing x value to 0.9, the Ms of $Zn_xNi_{1-x}Fe_2O_4$ nanorods decreases. The $Zn_{0.5}Ni_{0.5}Fe_2O_4$ nanorods show a maximum Ms of 51.1 emu/g.

When non-magnetic divalent Zn^{2+} ions are introduced, they tend to occupy tetrahedral(A) sites by transferring Fe^{3+} ions to

octahedral(B) sites due to their favoritism by polarization effect. However, site preference of cations also depends upon their electronic configurations. Zn^{2+} ions show marked preference for A sites where their free electrons respectively can form a covalent bond with the free electrons of the oxygen ion. This forms four bonds oriented towards the corners of a tetrahedron. Ni^{2+} ions have marked preference for an octahedral environment due to the favorable fit of the charge distribution of these ions in the crystal field at B sites. In view of the above considerations the cation distribution can be written as $(Zn_x^{2+}Fe_{1-x}^{3+})^A(Ni_{1-x}^{2+}Fe_{1+x}^{3+})^B$ [24,25]. As the content of Zn^{2+} ions increases, the number of Fe^{3+} ions on B-sites increases. Therefore the magnetic moment on B-site increases and the magnetic moment on A-sites decreases. The net value of M_s increases up to $x=0.5$. When 'x' exceeds 0.5, M_s starts decreasing because magnetic moment of the few Fe^{3+} ions on the A-site are no longer able to align all the moments on the B-sites antiparallel to themselves, since this is opposed by the negative B–B exchange interaction [26-29].

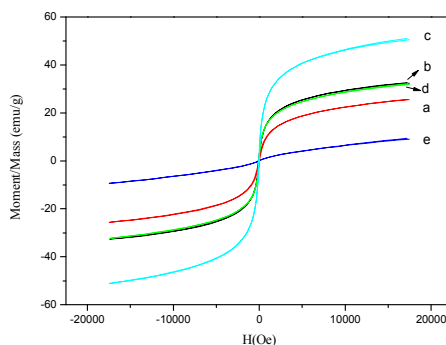


Fig. 8. Magnetic hysteresis loops for $Zn_xNi_{1-x}Fe_2O_4$ nanorods with different x values, (a) 0.1, (b) 0.35, (c) 0.5, (d) 0.65, and (e) 0.9.

Table 3. Magnetic parameters for $Zn_xNi_{1-x}Fe_2O_4$ nanorods

Sample	M_s (emu/g)
$Zn_xNi_{1-x}Fe_2O_4$ (x=0.1)	25.6
$Zn_xNi_{1-x}Fe_2O_4$ (x=0.35)	32.6
$Zn_xNi_{1-x}Fe_2O_4$ (x=0.5)	51.1
$Zn_xNi_{1-x}Fe_2O_4$ (x=0.65)	32.3
$Zn_xNi_{1-x}Fe_2O_4$ (x=0.9)	9.4

4. Conclusions

In summary, $\text{Zn}_{0.5}\text{Ni}_{0.5}\text{Fe}_2\text{O}_4$ nanorods were successfully prepared by calcination of the $\text{Zn}_{0.5}\text{Ni}_{0.5}\text{Fe}_2(\text{C}_2\text{O}_4)_3$ nanorods which were synthesized by a microemulsion method. The $\text{Zn}_{0.5}\text{Ni}_{0.5}\text{Fe}_2\text{O}_4$ nanorods retain the original rodlike morphology of the $\text{Zn}_{0.5}\text{Ni}_{0.5}\text{Fe}_2(\text{C}_2\text{O}_4)_3$ nanorods through the whole calcination process and they have the same dimension of 50–200 nm in diameter and several micrometers in length. The magnetic properties of the $\text{Zn}_{0.5}\text{Ni}_{0.5}\text{Fe}_2\text{O}_4$ nanorods are largely influenced by calcination temperatures. As the calcination temperatures increase from 350 to 900 °C, the M_s of the $\text{Zn}_{0.5}\text{Ni}_{0.5}\text{Fe}_2\text{O}_4$ nanorods increase. The $\text{Zn}_{0.5}\text{Ni}_{0.5}\text{Fe}_2\text{O}_4$ nanorods obtained at 900 °C show a maximum M_s of 77.1 emu/g. When the Zn doping level (x value) increases from 0.1 to 0.5, the M_s of samples increases. However with further increasing x value to 0.9, the M_s of $\text{Zn}_x\text{Ni}_{1-x}\text{Fe}_2\text{O}_4$ nanorods decreases.

Acknowledgement

This work was supported by National Natural Science Foundation of China (No. 21071017 and No. 21376029).

References

- [1] T. J. Shinde, A. B. Gadkari and P. N. Vasambekar, *J. Magn. Magn. Mater.*, 2013, **333**, 152.
- [2] E. P. Muniz, J. R. C. Proveti, R. D. Pereira, B. Segatto, P. S. S. Porto, V. P. Nascimento, M. A. Schettino and E. C. Passamani, *J. Mater. Sci.*, 2013, **48**, 1543.
- [3] P. Sivakumar, R. Ramesh, A. Ramanand, S. Ponnusamy and C. Muthamizhchelvan, *Mater. Res. Bull.*, 2011, **46**, 2204.
- [4] M. G. Naseri, E. B. Saion, H. A. Ahangar, M. Hashim and A. H. Shaari, *Powder. Technol.*, 2011, **212**, 80.
- [5] A. Ahlawat, V. G. Sathe, *J. Raman. Spectrosc.*, 2011, **42**, 1087.
- [6] P. Sivakumar, R. Ramesh, A. Ramanand, S. Ponnusamy and C. Muthamizhchelvan, *J. Mater. Sci. Mater. Electron.*, 2012, **23**, 1011.
- [7] R. H. Kodama, A. E. Berkowitz, E. J. McNiff and S. Foner, *Phys. Rev. Lett.*, 1996, **77**(2), 394.
- [8] J. Lopez, L. F. Gonzalez-Bahamon, J. Prado, J. C. Caicedo, G. Zambrano, M. E. Gomez, J. Esteve and P. Prieto, *J. Magn. Magn. Mater.*, 2012, **324**, 394.
- [9] J. Kalarus, G. Kogias, D. Holz and V. T. Zaspalis, *J. Magn. Magn. Mater.*, 2012, **324**, 2788.
- [10] A. P. Kazin, M. N. Rumyantseva, V. E. Prusakov, I. P. Suzdalev and A. M. Gaskov, *J. Solid. State. Chem.*, 2011, **184**, 2799.
- [11] S. Marins, T. Ogasawara and L. Tavares, *J. Mater. Sci.*, 2011, **46**, 1640.
- [12] K. Gheisari, S. D. Bhame, J. T. Oh and S. Javadpour, *J. Supercond. Nov. Magn.*, 2013, **26**, 477.
- [13] C. Caizer, *Mat. Sci. Eng. B-Solid.*, 2003, **100**, 63.
- [14] A. Ceylan, S. Ozcan, C. Ni and S. I. Shah, *J. Magn. Magn. Mater.*, 2008, **320**, 857.
- [15] S. M. Olhero, D. Soma, V. S. Amaral, T. W. Button, F. J. Alves and J. M. F. Ferreira, *J. Eur. Ceram. Soc.*, 2012, **32**, 2469.
- [16] M. Sertkol, Y. Koseoglu, A. Baykal, H. Kavas and A. C. Basaran, *J. Magn. Magn. Mater.*, 2009, **321**, 157.
- [17] Z. Yue, W. Guo, J. Zhou, Z. Gui and L. Li, *J. Magn. Magn. Mater.*, 2004, **270**, 216.
- [18] M. Rahimi, P. Kameli, M. Ranjbar, H. Hajihashemi and H. Salamati, *J. Mater. Sci.*, 2013, **48**, 2969.
- [19] K. Gheisari, S. Shahriari and S. Javadpour, *J. Alloy. Compd.*, 2013, **552**, 146.

- [20] H. Y. Wu, Q. Z. Jiao, Y. Zhao, H. B. Liu, X. F. Li, Y. Cao and X. L. Tang, *Synth. React. Inorg. M.*, 2010, **40**, 695.
- [21] A. Verma, T. C. Goel, R. G. Mendiratta and M. I. Alam, *Mater. Sci. Eng. B*, 1999, **60**, 156.
- [22] Z. T. Zhang, A. J. Rondinone, J. X. Ma, J. Shen and S. Dai, *Adv. Mater.*, 2005, **17**, 1415.
- [23] M. Rajendran, R. C. Pullar, A. K. Bhattacharya, D. Das, S. N. Chintalapudi and C. K. Majumdar, *J. Magn. Magn. Mater.*, 2001, **232**, 71.
- [24] A. D. Sheikh, V. L. Mathe, *J. Mater. Sci.*, 2008, **43**, 2018.
- [25] M. Ajmal, A. Maqsood, *Mater. Lett.*, 2008, **62**, 2077.
- [26] E. W. Gorter, *Nature*, 1950, **165**, 798.
- [27] C. W. Yan, Q. S. Zeng, G. F. Goya, T. Torres, J. F. Liu, H. P. Wu, M. Y. Ge, Y. W. Zeng, Y. W. Wang and J. Z. Jiang, *J. Phys. Chem. C*, 2007, **111**, 12274.
- [28] M. A. Ahmed, M. M. El-Sayed, *J. Magn. Magn. Mater.*, 2007, **308**, 40.
- [29] J. T. Wu, N. Li, J. Xu, Y. Q. Jiang, Z. G. Ye, Z. X. Xie and L. S. Zheng, *Appl. Phys. Lett.*, 2011, **99**, 202505.